Method for Tracking the Evolution of Fatigue Cracks in Rail Turnouts Using Ultrasonic Guided Waves

SHUO XIA, FUZAI LV, ZHIFENG TANG
and PENGFEI ZHANG

ABSTRACT

Rail turnouts are an essential component of railway systems, and rail bottom is prone to fatigue cracks under long-term exposure to heavy loads, which can lead to structural failure and pose a serious threat to train operation safety. Since fatigue crack propagation is nonlinear and concealed, early detection is of great significance. Ultrasonic guided waves, due to their advantages of long propagation distance, low attenuation, and ability to detect concealed areas, are widely used in structural health monitoring. However, during the early stages of crack propagation, the cracks are extremely small, and the signal features can be easily obscured by noise, significantly complicating reliable detection. This paper proposes a virtual sensor-based anomaly feature extraction method, in which ultrasonic guided wave signals are segmented into sliding window subsequences serving as multiple virtual sensors. By combining temporal features and fluctuation patterns, the anomaly weight of each subsequence is evaluated to identify potential abnormal regions. Validation through a switch rail fatigue loading experiment demonstrates that the proposed method can effectively track crack development trends at the early stages, adapt to complex signal scenarios, and significantly improve the accuracy and reliability of structural health monitoring.

INTRODUCTION

Globally, the development of modern railway systems has been increasingly shaped by the expansion of high-speed passenger rail and heavy-haul freight transport. By 2022, the total operational length of high-speed rail lines worldwide had reached nearly 60,000 kilometers, underscoring the rapid pace of growth in this sector. Rail turnouts, which enable trains to transition between tracks, represent critical infrastructure components. However, they are also among the most failure-prone elements, as illustrated in Figure 1. The switch rail, a movable part of the turnout, is subjected to severe cyclic loading during operation. The maximum stress typically concentrates at the rail bottom, rendering this region particularly susceptible to transverse fatigue cracks [1]. Once initiated, such cracks can propagate rapidly under cyclic loading, potentially leading to catastrophic failure. In documented cases of turnout failures, the majority have been attributed to transverse fatigue cracks originating at the rail bottom [2]. As a result, the early detection and continuous monitoring of these cracks in switch rails have become key priorities in ensuring railway safety and reliability [3–6].

Ultrasonic guided wave (UGW) monitoring, as an advanced non-destructive testing technique, has demonstrated significant advantages in the field of structural health

Shuo Xia, School of Mechanical Engineering, Zhejiang University, Hangzhou, 310058, China
Fuzai Lv, School of Mechanical Engineering, Zhejiang University, Hangzhou, 310058, China
Zhifeng Tang, College of Biomedical Engineering and Instrument Science, Zhejiang University, Hangzhou, 310027, China
Pengfei Zhang, Hangzhou Zheda Jingyi Electromechanical Technology Corporation Ltd., Hangzhou, 311121, China

monitoring (SHM) [7–11]. This technology enables efficient inspection of large-scale structures from a single excitation point, with detection ranges extending up to several tens of meters. It is particularly effective for identifying defects in hidden or inaccessible regions, such as pipelines, rails, cables, and steel plates. Moreover, UGW monitoring can be used for real-time structural assessment, supporting data-driven preventive maintenance strategies. With its high efficiency, sensitivity, and real-time capabilities, UGW monitoring holds great potential for widespread application in SHM [12].

Fatigue crack propagation exhibits a highly nonlinear behavior. In the early stages, crack growth is relatively slow and generally follows the power-law relationship described by Paris' law [13]. However, once the crack reaches a critical size, its propagation rate increases dramatically, potentially leading to structural failure. Due to the small size of early-stage cracks, UGW signals are extremely weak and can be easily obscured by environmental noise and background interference. As the crack enters the macro-propagation stage, the structure's residual strength declines sharply, and the risk of failure rises rapidly. This combination of low detectability in early stages and accelerated progression in later stages challenges traditional monitoring approaches and poses significant risks to operational safety. The strong nonlinearity of crack propagation thus highlights the urgent need for effective early-stage monitoring [14]. Consequently, the development of highly sensitive detection technologies has become a key focus in ensuring the reliability and safety of critical infrastructure.

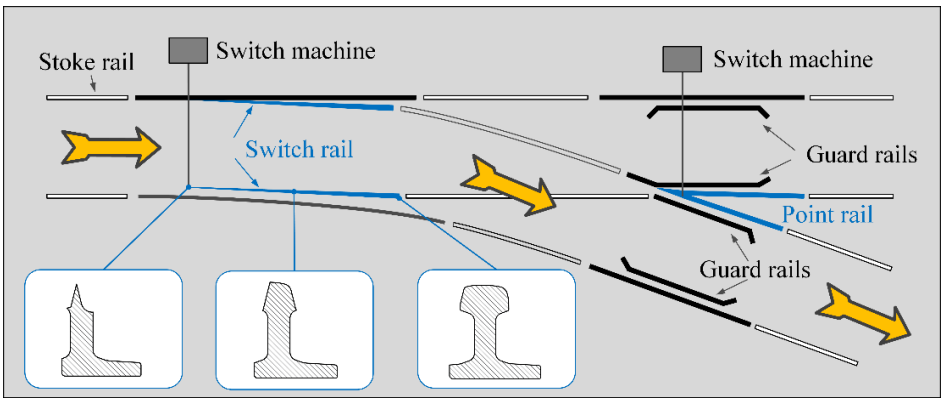

Figure 1. Schematic Diagram of a Rail Turnout

An in-depth analysis of UGW signal characteristics during fatigue crack initiation and propagation shows that minor damage, such as micro-cracks, induces a localized increase in echo amplitude. This change is unidirectional and irreversible [15]. Leveraging this characteristic, this study proposes a virtual sensor-based anomaly feature extraction method (VSAFE) for early fatigue crack detection. In VSAFE, the monitoring signal is first divided into multiple subsequences using a sliding window approach. Each subsequence is then locally matched to a baseline signal using cosine similarity, effectively mitigating temperature-induced variations. Subsequently, each window is treated as a virtual sensor, and its extracted features are considered as corresponding sensor data. By assigning weights to virtual sensors based on historical

data—emphasizing those exhibiting abnormal behavior indicative of fatigue cracks—the method enables sensitive detection and early warning of micro-cracks.

METHODOLOGY

SHM of turnouts involves analyzing the relationship between the baseline signal (BS) $B(x)$ and the monitoring signal (MS) $M(x)$ to extract information. Initially, BS is divided into segments $b(x)$ using a sliding window, with each window containing a local subsequence $m(x)$ of MS. Then, the local similarity between the two sequences is calculated by sliding the corresponding local subsequence of BS through the window. This relationship is quantified by cosine similarity as follows:

$$\sin(n) = \frac{\sum_{i=1}^{n} m(x_i) b(x_i + n)}{\sqrt{\sum_{i=1}^{n} m^2(x_i)} \sqrt{\sum_{i=1}^{n} b^2(x_i + n)}}, \tag{1}$$

where n in $b^2(x_i + n)$ indicates that MS segment is matched to the corresponding local region of BS within a limited sliding range $\pm n$. The sliding process involves comparing the similarity values across all positions to determine the location with the highest similarity, thereby identifying the optimal matching position of MS segment relative to BS. The resulting offset, $n_{\max}$, represents the degree of local lead or lag in the signal. This method compensates for local signal shifts and effectively mitigates phase variations caused by temperature changes.

After obtaining the MS window subsequence and its best-matched BS subsequence, the relative energy difference between the two is computed. This difference reflects the extent of dynamic variation in the MS signal within the local region. The process condenses the local temporal characteristics into a scalar feature, enabling the extraction of information indicative of localized structural changes. This computation is expressed as:

$$u = \frac{\sum_{i=1}^{n} [m(i)^2 - b(i)^2]}{\sum_{i=1}^{n} b(i)^2}, \tag{2}$$

where u is considered the response signal received by the "virtual transducer" at this position.

The entire MS sequence is traversed using a sliding window, with the above process repeated to construct an array of signals from multiple "virtual transducers" in a time sequence $\boldsymbol{U}(t) = \left[\boldsymbol{u}_1(t) \quad \boldsymbol{u}_2(t) \quad \cdots \quad \boldsymbol{u}_k(t)\right]$. This virtual sensor array emulates multi-point simultaneous monitoring, offering comprehensive spatio-temporal information essential for health status assessment and damage detection.

When a defect occurs in the structure, the signal received by the virtual sensor at the corresponding position exhibits significant anomalies, and the overall signal trend also changes. However, due to potential noise, it is necessary to preprocess the response

signals from each virtual sensor before feature analysis. In this study, a filtering method is applied to denoise the signals, effectively suppressing the impact of noise and improving the accuracy of anomaly detection. The expression is:

$$\bar{\boldsymbol{U}}_t = \alpha \boldsymbol{U}_t + (1-\alpha)\bar{\boldsymbol{U}}_{t-1}, \tag{3}$$

where α is the signal smoothing factor, used to eliminate high-frequency noise, and is typically set between 0.05 and 0.1.

After filtering, feature extraction is performed, which is carried out along two dimensions: spatial and temporal. The spatial dimension features aim to analyze the response differences among all virtual sensors at the same moment. By measuring the relative anomaly degree between sensors, the Spatial Anomaly Intensity (SAI) index is constructed, as shown:

$$\mathrm{SAI} = \frac{\bar{\boldsymbol{U}}_t - \max(\bar{\boldsymbol{U}}_0)}{\max(\bar{\boldsymbol{U}}_t) + \max(\bar{\boldsymbol{U}}_0)}, \tag{4}$$

where the initial value and the currently collected value are used as references, allowing for a thorough assessment of the spatial anomalies in the signal.

The temporal dimension features focus on the historical response changes of a single virtual sensor over time, identifying its anomalous trends. This allows for the calculation of the Temporal Anomaly Intensity (TAI) index, as shown:

$$\mathrm{TAI} = \sigma\left(q \cdot \frac{(1-p)\bar{\boldsymbol{U}}_t - (1+p)\bar{\boldsymbol{U}}_0}{\bar{\boldsymbol{U}}_t + \bar{\boldsymbol{U}}_0} \right), \tag{5}$$

where $\sigma(\bullet)$ represents the sigmoid function, which is used to extract spatial anomaly features. p and q are two adjustable parameters that dynamically control the sensitivity of anomaly detection. Typically, p is chosen between 0.5 and 0.7, while q ranges from 8 to 12.

Finally, by combining the SAI and TAI, a comprehensive anomaly assessment metric, the Anomaly Score (AS), is obtained, as shown:

$$\mathrm{AS} = \mathrm{SAI} \cdot \mathrm{TAI} \tag{6}$$

AS is a spatiotemporal state matrix that fully records all spatial and temporal information from the start of monitoring to the current moment, providing a comprehensive representation of the state evolution. To achieve defect localization and quantification, this study uses the maximum anomaly assessment metric among all virtual sensors as the Damage Index (DI) $\mathrm{DI} = \max(\mathrm{AS})$, and the corresponding monitoring position of this virtual sensor is identified as the region where the structural defect has occurred.

EXPERIMENTAL SETUP

To validate the effectiveness of VSAFE, an experiment was designed to simulate fatigue crack initiation and propagation in the switch rail of a railway turnout. The experimental setup is illustrated in Figure 2. A 60AT2 switch rail model, 5 m in length, was used. One end was fixed to the sleeper using fastener bolts, while the other remained free to mimic field conditions. The rail bottom, known as a critical stress concentration zone, was selected as the target region for crack initiation. To simulate real-world loading conditions, a vertical cyclic load was applied at the rail head to induce localized stress and promote crack development at the rail bottom.

To simulate crack initiation, a stress concentration groove was machined 2500 mm from one end of the 60AT2 rail to induce and propagate fatigue cracks. Cyclic loading was applied using a four-channel electro-hydraulic servo system, as shown in Figure 2. The load acted vertically on the upper surface of the rail head. The system operated at a frequency of 4 Hz with a load amplitude of 300 kN, simulating the cyclic stress typical of train passage.

Four strain gauges were installed on the rail bottom to monitor the crack. Additionally, an ultrasonic flaw detector was used to perform point-by-point crack detection in the stress concentration area, providing supplementary verification of the monitoring. The UGW excitation and reception were handled by UGW monitoring system, which has a sampling frequency of 1 MHz. A magnetostrictive patch transducer (MPT) was placed at rail bottom, responsible for the bidirectional conversion between electromagnetic and mechanical energy. MPT features excellent directional and frequency response characteristics, making it suitable for exciting and receiving UGW in rails. The excitation signal was a 4-cycle sine wave modulated with a Hanning window, set to a frequency of 55 kHz to ensure good propagation performance and defect sensitivity of the excited UGW mode.

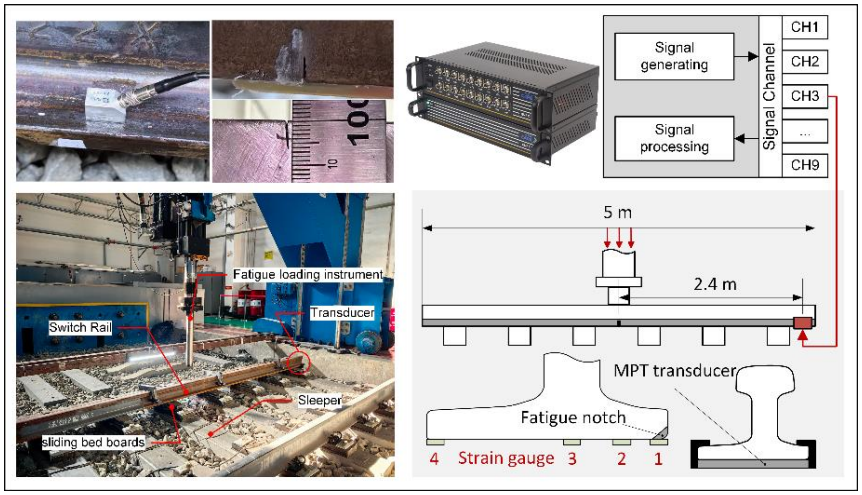

Figure 2. Experimental setup

RESULTS AND ANALYSIS

The total loading cycles from the start to the fracture of the switch rail was 744 thousand loading cycles (kLC). Figure 3 shows the data from the strain gauges and ultrasonic testing at different cycle counts. Strain gauge 1 showed an increase in strain at 165 kLC and failed at 319 kLC, suggesting early damage at this location. Strain gauge 2 showed a change at 694 kLC and failed at 744 kLC. Strain gauges 3 and 4 exhibited minimal fluctuations and failed simultaneously at 744 kLC when the switch rail fractured, indicating later damage. The strain values reflect stress differences along the rail bottom: higher stress on the short leg side and lower stress on the long leg side.

Ultrasonic testing first detected the crack at 535 kLC, with a length of 12.1 mm. The crack then rapidly propagated, leading to fracture at 744 kLC when the crack reached 21.5 mm. Based on the data from strain gauge 1 and ultrasonic testing, it can be inferred that the macroscopic crack propagation occurred between the 165 kLC and 535 kLC of loading.

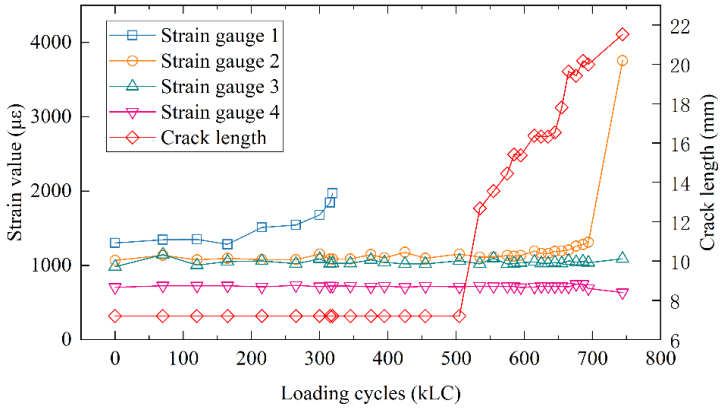

Figure 3. Strain gauge data and fatigue crack length measured by ultrasonic testing

Based on VSAFE, AS results are obtained as shown in Figure 4, which include both spatial and temporal information of fatigue crack propagation. In Figure 4, two adjacent color bands can be observed, displaying a color transition from blue to red. The longer color band corresponds to the signal received by the 247th virtual transducer, with the anomaly first appearing at 360 kLC. The shorter color band represents the signal from the 240th virtual transducer, where the anomaly initiated after 365 kLC.

The close correlation between the two color bands reflects the multimodal phenomenon of UGW propagating in the rail. Both modes exhibit notable energy and respond to the fatigue crack. The energy distribution between these modes differs, leading to a temporal difference in the appearance of the two color bands. Furthermore, the absence of anomalous signals in the remaining regions of the color map indicates that these structural components remain in a healthy state. Based on the relationship between the virtual sensors and the switch rail position, the fatigue crack location can be calculated to be 2470mm from MPT, with an error margin of 70 mm.

Figure 5 shows the comparison between the proposed method, strain gauge 1, and ultrasonic testing. The strain gauge 1 primarily records the strain magnitude at the rail bottom crack, with its values normalized to the range of 0.7 to 1 for comparative analysis. DI begins to rise at 359 kLC, indicating that the method has successfully detected the anomaly associated with fatigue crack initiation, which aligns with the fatigue crack growth period identified in the previous analysis. Subsequently, DI value continuously increases, ultimately reaching its maximum value of 0.96 at the point of rail fracture.

The experimental results show that while VSAFE exhibits slightly lower sensitivity compared to strain gauges, it significantly outperforms traditional ultrasonic testing methods. However, in practical engineering applications, it is impractical to deploy strain gauges extensively on the rail bottom due to significant challenges in both installation and maintenance. Consequently, the proposed method demonstrates excellent applicability and engineering advantages in practical detection processes.

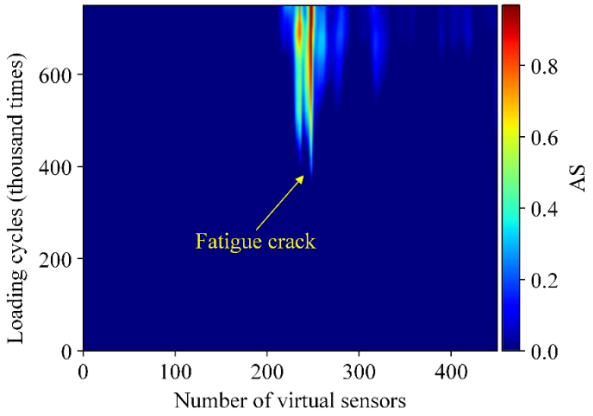

Figure 4. Color map of AS

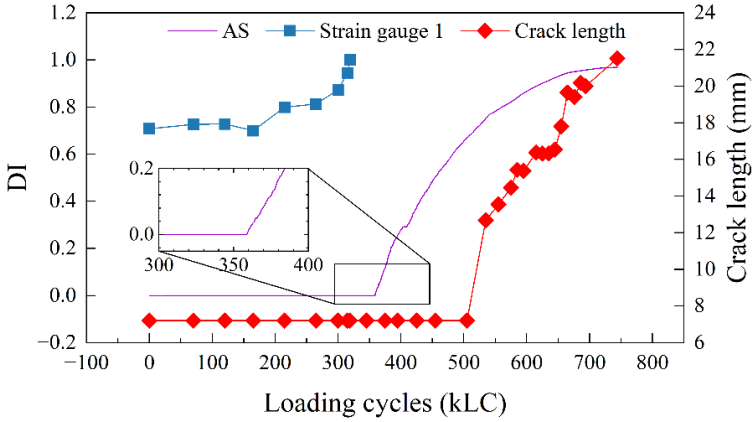

Figure 5. The comparison between the proposed method, strain gauge 1, and ultrasonic testing.

CONCLUSION

To address the challenges in monitoring fatigue cracks in high-speed railway turnouts, this study proposes VSAFE for switch rail SHM, based on experimental

investigations. The results demonstrate that VSAFE can effectively capture signal variations during crack propagation and enable early-stage crack tracking. Although its sensitivity is slightly lower than that of strain gauges, VSAFE offers superior performance in terms of detection range, ease of installation, and adaptability to operational conditions, compared to traditional ultrasonic testing and point-wise strain monitoring techniques. These advantages highlight its potential for enhancing railway safety while reducing reliance on manual inspection, thus contributing to cost-effective and automated SHM solutions.

Future work could focus on refining the signal processing algorithms to improve crack type classification accuracy and integrating multimodal sensing strategies to enhance the system's overall assessment capabilities.

REFERENCES

1. Yi, Q., X. Liu, S. Wang, H. Chang, Z. Jiang, and W. Wang. 2025. Failure mechanism and crack propagation behavior of turnout stock rail in high-speed railway, *Engineering Failure Analysis*, 167:109026.
2. Zerbst, U., M. Madia, C. Klinger, D. Bettge, and Y. Murakami. 2019. Defects as a root cause of fatigue failure of metallic components. I: Basic aspects, *Engineering Failure Analysis*, 97:777–792.
3. Li, D.-H., D.-G. Shang, L. Xue, M. E. Barkey, and H. Chen. 2020. Real-time damage evaluation method for multiaxial thermo-mechanical fatigue under variable amplitude loading, *Engineering Fracture Mechanics*, 229:106948.
4. Stopka, K. S. and D. L. McDowell. 2020. Microstructure-sensitive computational multiaxial fatigue of Al 7075-T6 and duplex Ti-6Al-4V, *International Journal of Fatigue*, 133:105460.
5. Fatemi, A., R. Molaei, and N. Phan. 2020. Multiaxial fatigue of additive manufactured metals: Performance, analysis, and applications, *International Journal of Fatigue*, 134:105479.
6. Sun, J. and H. Yuan. 2019. Life assessment of multiaxial thermomechanical fatigue of a nickel-based superalloy Inconel 718, *International Journal of Fatigue*, 120:228–240.
7. Lyu, F., X. Zhou, Z. Ding, X. Qiao, and D. Song. 2024. Application research of ultrasonic-guided wave technology in pipeline corrosion defect detection: A review, *Coatings*, 14(3):358.
8. Zheng, Y., S. Wang, P. Zhang, T. Xu, and J. Zhuo. 2022. Application of nondestructive testing technology in quality evaluation of plain concrete and RC structures in bridge engineering: A review, *Buildings*, 12(6):843.
9. Su, Z., L. Ye, and Y. Lu. 2006. Guided Lamb waves for identification of damage in composite structures: A review, *Journal of sound and vibration*, 295(3-5):753–780.
10. Wang, X., M. Lin, J. Li, J. Tong, X. Huang, L. Liang, Z. Fan, and Y. Liu. 2022. Ultrasonic guided wave imaging with deep learning: Applications in corrosion mapping, *Mechanical Systems and Signal Processing*, 169:108761.
11. Tabjula, J., S. Kanakambaran, P. Rajagopal, and B. Srinivasan. 2023. Sparse sampled visualization of ultrasonic guided waves for defect identification in plate structures, *NDT & E International*, 138:102890.
12. Abbas, M. and M. Shafiee. 2018. Structural health monitoring (SHM) and determination of surface defects in large metallic structures using ultrasonic guided waves, *Sensors*, 18(11):3958.
13. Yuan, L. and Y. Wei. 2024. Unified SIF at different stress ratios and the physical insight on the exponent of the Paris law, *International Journal of Fatigue*, 184:108314.
14. Wang, P., L. Ye, X. Liu, Y. Dong, and L. Zhao. 2023. Effects of grain structures on fatigue crack propagation behavior of an Al-Cu-Li alloy, *International Journal of Fatigue*, 177:107927.
15. Wang, Y., F. Song, Q. Feng, W. Qiao, S. Dong, Y. Jiang, and Q. Ma. 2024. Basic Theory and Applications of Oil and Gas Pipeline Non-Destructive Testing Methods, *Energies*, 17(24):6366.